IEEE Access
Multidisciplinary ⋮ Rapid Review ⋮ Open Access Journal

Received 31 March 2023, accepted 16 April 2023, date of publication 24 April 2023, date of current version 1 May 2023.

Digital Object Identifier 10.1109/ACCESS.2023.3269578

RESEARCH ARTICLE

Adaptive Control Strategy for Three-Phase Three-Level T-Type Rectifier Based on Online Disturbance Estimation and Compensation

ALI SHARIDA[1,2], (Student Member, IEEE), SERTAC BAYHAN[3,4], (Senior Member, IEEE), AND HAITHAM ABU-RUB[1], (Fellow, IEEE)

[1]Department of Electrical and Computer Engineering (ECEN), Texas A&M University at Qatar, Doha, Qatar
[2]Department of Electrical and Computer Engineering (ECEN), Texas A&M University, College Station, TX 79016, USA
[3]Qatar Environment and Energy Research Institute, Hamad Bin Khalifa University, Doha, Qatar
[4]Department of Electrical-Electronic Engineering, Gazi University, 06560 Ankara, Turkey

Corresponding author: Ali Sharida (ali.sharida@qatar.tamu.edu)

This work was supported by the Qatar National Research Fund (a member of Qatar Foundation) under Grant NPRP12C-33905- SP-213.

ABSTRACT This paper proposes an adaptive control technique (ACT) for a three-phase, three-level, T-type rectifier based on online disturbance estimation and compensation. The proposed solution also regulates the DC-link voltage and grid currents under uncertainties, disturbances, measurement noises, and unbalanced grid voltages without cascaded control. The proposed controller consists of two layers; the first one is responsible for estimating nonlinearities and model uncertainties based on Kalman Filter Algorithm (KFA). The second layer is responsible for controlling both grid currents and DC link voltage using Linear Quadratic Regulator (LQR). The proposed controller is analyzed theoretically, validated experimentally, and the performance of the proposed controller is compared with two other controllers. The simulation and experimental results prove the superiority of the proposed controller and show that the proposed controller can ensure fast-tracking performance with almost zero steady-state error. The proposed controller has the ability to overcome severe disturbances such as AC and DC side disturbances, measurement noises, and mathematical model's uncertainties even up to 400%.

INDEX TERMS Three-level T-type rectifier, online disturbance estimation, adaptive control, Kalman filter, LQR control, single-loop control.

I. INTRODUCTION

Controlled rectifiers are widely used in many industrial applications, such as DC drives, controlled power supply, wireless power transfer, and electric vehicle battery chargers [1], [2], [3], [4], [5]. Controlled rectifiers have attracted many researchers worldwide due to their advantages represented by the ability to control the output DC voltage, produce sinusoidal line currents, and ensure the operation at the unity power factor.

Controlled rectifiers can be voltage source [6] or current source [7], [8]. The significant drawbacks of the current source type are that it has low efficiency and causes a distortion in the grid current. On the other hand, the voltage source rectifier has a simple structure and can be controlled easily [9].

The controlled rectifier can be either two-level or multilevel. Recently, multilevel converters have been used as alternatives to the two-level in medium and high voltage applications due to their many advantages [10], such as high power quality and higher efficiency. The multilevel converters can be built through different topologies such as neutral point clamped (NPC) [11], flying capacitor [12], active NPC [13], cascaded H-bridge rectifier [14], packed-U-cell [15], and T-type [10]. The T-type rectifier has multiple advantages over its counterparts, such as low power losses, reduced components count, simple control, and higher efficiency [10].

The associate editor coordinating the review of this manuscript and approving it for publication was Reinaldo Tonkoski.

TABLE 1. List of symbols.

Symbol	Description
$\mathbf{V}_{abc}$	Vector of grid voltages
$\mathbf{I}_{abc}$	Vector of grid currents
$\mathbf{u}_{abc}$	Vector of poles' voltages
L	Input filter inductance
R	Filter's internal resistance
C_1 , C_2	DC side capacitance
$\mathbf{V}_{dq}$	Vector of grid voltages in *dq* frame
$\mathbf{I}_{dq}$	Vector of grid currents in *dq* frame
$\boldsymbol{\xi}$	Vector of disturbances
$\mathbf{A}$	Continuous states matrix
$\mathbf{B}$	Continuous input matrix
$\mathbf{A}_e$	Continuous extended states matrix
$\mathbf{B}_e$	Continuous extended input matrix
$\mathbf{A}_{ed}$	Discrete extended states matrix
$\mathbf{B}_{ed}$	Discrete extended input matrix
$\mathbf{x}_{ek}$	Discrete extended states vector
$\hat{\mathbf{x}}_{ek}$	Estimated extended states vector
T_s	Sampling time
$\mathbf{e}_{dq}$	Current tracking error in *dq* frame
LQR	Linear quadratic tracker
KFA	Kalman Filter Algorithm
ACT	Adaptive Control Technique
PBC	Passivity-Based Control
H∞	H of Inifinity controller
$\mathbf{K}$	LQR gain matrix
V_{dc}	DC link voltage
V^*_{dc}	DC link voltage reference
R_L	Load resistance
ΔV_c	Voltage difference between DC side capacitors' voltages.

These advantages have attracted many researchers from around the world to adopt this topology [16]. Thus, multiple control algorithms have been proposed in the past to control the T-Type rectifier. These controllers aim to control and improve different criteria such as DC link voltage regulation, line currents overshoot, total harmonics distortion (THD), and input power factor. The basic principle of these controllers is to compute the reference line currents based on the error of the DC link voltage. Then, the line current can be controlled using different control strategies called Direct Current Control (DCC) [17]. A Direct Power Control (DPC) mechanism was also employed to regulate the output voltage of the DC link [16].

DCC and DPC methods depend entirely on the dynamic model to perform decoupling between the current elements in the *dq* frame. However, in industrial applications, the controlled rectifiers are exposed to disturbances and uncertainties, where the coupling effects cannot be neglected and cannot be compensated mathematically. This leads to imperfect decoupling between current components, which would increase the error in DC link voltage regulation and deteriorate the response of the current controller.

To overcome the aforementioned problems, multiple advanced controllers were proposed, such as Model Predictive Control (MPC), Sliding mode controller (SMC), and Fuzzy Logic controller (FLC). MPC is an effective control algorithm that depends on the mathematical model to predict the response of the rectifier over a horizon [18]. However, such approach has two limitations; it requires a well-defined model, and it consumes high computational time, especially for longer horizons [19]. Multiple researchers employed Fuzzy logic controllers to perform the control tasks [20]. However, fuzzy logic controllers mainly suffers from the lack of a systematic method to set the rules or the memberships.

KFA is used in [21] to design an adaptive controller based on dual-division-summation (DDS) current control. The KFA is used to estimate filter's inductance and grid impedance. The estimated parameters are then used to tune the gains of the controller. However, the proposed method requires three algorithms, DDS control algorithm, grid impedance and filter inductance estimator, and gain correction algorithm. This increases the complexity of the controller and the computational load of the entire control algorithm. Moreover, multiple requirements (such as voltage controller and reference current generation) must be added to the proposed method to make it suitable for voltage-controlled applications. This adds extra complexity and computational load.

A sliding mode controller (SMC) was proposed in [10] to control the line current of a three-phase T-type rectifier. The controller was designed to achieve three main tasks, DC link voltage regulation, unity power factor, and DC capacitors voltages balance. Such a controller shows an excellent steady-state response under unbalanced grid voltage and an excellent transient response even when the load is changed suddenly. However, the proposed SMC is exposed to chattering which may deteriorate the tracking accuracy and generates unmodeled high frequency dynamics. Moreover, the proposed SMC requires a cascaded loop for current DC link voltage regulation. The drawbacks of the cascaded control are the slow response time, increased complexity of the controller, and increased number of tuned parameters. KFA and SMC are employed in [22] and [23] to achieve an adaptive control of a grid connected inverter. In [22] KFA is used to estimate the states of inverter's model. The estimated states are used to design three independent current sliding mode controllers. However, the sliding mode controller is exposed to chattering. Moreover, an online design of three independent sliding mode controllers is complex and time consuming. In [23], KFA is used for reducing the number of sampling sensors, while a fuzzy-fractional-order nonsingular terminal SMC (FFO-SMC) is used for robust control. This method is robust, has satisfactory steady state and dynamic response, and deals with chattering problem, however, it has two drawbacks. The first one, FFO-SMC depends on the derivatives of the grid voltage and the reference current. The identification of states drivatives is highly affected by measurement noise, which may lead to system unstability. The second drawback is that the FFO-SMC method contains five different gains that need

tuning and have high impact on the controller's response. Underestimating any gain will deteriorate the response of the controller.

The integration between KFA and MPC was proposed in [24] to design a current controller for unbalanced grid-connected inverter. The positive and negative sequence components of the grid voltage were extracted by KFA, while MPC was employed to regulate the currents of the grid. In fact, MPC is considered one of the most time-consuming controllers, and the addition of KFA to the MPC makes the computational load even worse.

A passivity-base control (PBC) [25] was proposed to control a single-phase T-type rectifier. The major advantage of this method is the usage of a single control loop to control the entire system. This advantage simplifies the design of the controller, reduces the computation time, and increases the response performance compared to cascaded control. However, the DC link voltage feedback was not included in the proposed control technique to regulate the DC link voltage. The regulation of the DC link voltage is achieved based on the balanced power principle between the input and the output. In practical application, there are multiple sources of losses, such as switching losses, conduction losses, and losses during transients. These losses may lead to steady-state errors. H-of-infinity ($H\infty$) controller was also proposed as an adaptive disturbance rejection controller [26]. This method depends on two cascaded loops to achieve the DC link voltage and grid currents control task. The inner loop represents an adaptive DC link voltage regulator, while outer loop is an $H\infty$-based grid currents controller. This controller performs disturbance rejection task due to the robust nature of the $H\infty$ controller, where the superiority of this method over traditional extended state observers (ESO) is proved. However, the proposed method has many constants to be tuned and there is no systematical method to tune them. Underestimating the effect of tuning these parameters deteriorates the response of the controller especially during transient periods. As the objectives of [25] and [26] are considered in this paper, they were adopted in the comparison study to prove the superiority of the proposed controller.

This paper proposes a two-layer adaptive control algorithm for a three-phase, three-level, T-type rectifier. The proposed controller depends on separating the dynamic model into two parts. The first one contains the linear, well-known, and decoupled terms, while the second part contains the unknown, coupled, and non-linear terms. As the first part consists of the linear and decoupled terms only, it can be controlled directly using any linear controller such as Proportional Integral (PI) controller, Linear Quadratic Regulator (LQR), and State Feedback (SFB) controller. The second part of the dynamic model was considered a disturbance and assumed to be completely unknown. To compensate the effects of the unknown terms, they are considered as a lumped disturbance vector. Then, this vector is inserted into the system as unmeasured states. These states are estimated using KFA and added directly to the results of the linear controller.

The controller is designed to obtain satisfactory performance even if the uncertainty in the model is severe, which is the main contribution of the paper. The proposed controller also provides the following advantages,

1. Depends on a single control loop instead of the cascaded control loop. A single control loop increases the response performance compared to a cascaded loop and simplifies the design of the controller.
2. Requires tuning for only one gain related to DC side capacitors' voltage balancing, while the control law (LQR) consists of unity gains, and the KFA can automatically tune its gains based on the error between the measured and the estimated values.
3. A smooth transient is guaranteed regardless of the amount of uncertainty, the abnormal conditions, and reference step size, thanks to the adaptive generation of the reference signals.
4. The proposed controller is robust against severe parameter mismatches, measurement noises, and abnormal grid conditions, such as unbalanced and distorted grid voltages.

The rest of the paper is organized as follows; dynamic modeling of the T-type rectifier is introduced in section II. The design of the controller is described in section III. Comparison study and experimental results are shown in section IV. Finally, the paper is concluded in section V.

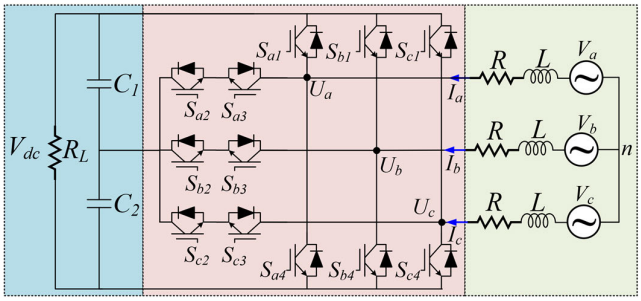

FIGURE 1. Three-phase three-level T-type rectifier circuit diagram.

II. MATHEMATICAL MODEL OF T-TYPE RECTIFIER

Fig. 1 shows the circuit diagram of a three-phase three-level T-type rectifier. It has two capacitors on the DC side (C_1 and C_2), and three legs connected to the grid through inductor-filters (L) which has an internal resistance (R). Each leg consists of four power switches, their gates (S_{ij}) are controlled using the traditional three-level switching function. Such function consists of two carrier signals with a constant offset (+1) in their amplitudes. The AC side of the rectifier is modeled as follows [10],

$$\mathbf{V}_{abc} = L\frac{d\mathbf{I}_{abc}}{dt} + R\mathbf{I}_{abc} + \mathbf{u}_{abc} \tag{1}$$

To reduce the number of controlled states, (1) can be written in the dq frame as follows [27],

$$V_d = RI_d + L\frac{dI_d}{dt} - \omega LI_q + u_d \tag{2}$$

$$V_q = RI_q + L\frac{dI_q}{dt} + \omega LI_d + u_q \tag{3}$$

or in state space representation as follows,

$$\underbrace{\begin{bmatrix}\dot{I}_d\\ \dot{I}_q\end{bmatrix}}_{\dot{\mathbf{x}}} = -\underbrace{\begin{bmatrix}\frac{R}{L} & 0\\ 0 & \frac{R}{L}\end{bmatrix}}_{\mathbf{A}}\underbrace{\begin{bmatrix}I_d\\ I_q\end{bmatrix}}_{\mathbf{x}} - \underbrace{\begin{bmatrix}\frac{1}{L} & 0\\ 0 & \frac{1}{L}\end{bmatrix}}_{\mathbf{B}}\begin{bmatrix}u_d\\ u_q\end{bmatrix} + \underbrace{\begin{bmatrix}\frac{V_d}{L} + \omega I_q\\ \frac{V_q}{L} - \omega I_d\end{bmatrix}}_{\xi} \tag{4}$$

(4) represents a first-order coupled linear system. Therefore, the system cannot be controlled by a linear controller directly due to the coupling effects between the states I_d and I_q. To use the KFA, the disturbances should be augmented with system states as an extended state; therefore, (4) can be written as follows,

$$\underbrace{\begin{bmatrix}\dot{I}_d\\ \dot{I}_q\\ \dot{\xi}\end{bmatrix}}_{\dot{\mathbf{x}}_e} = \underbrace{\begin{bmatrix}\mathbf{A} & \mathbf{I}_2\\ \mathbf{0}_{2\times2} & \mathbf{0}_{2\times2}\end{bmatrix}}_{\mathbf{A}_e}\underbrace{\begin{bmatrix}I_d\\ I_q\\ \xi\end{bmatrix}}_{\mathbf{x}_e} + \underbrace{\begin{bmatrix}\mathbf{B}\\ \mathbf{0}_{2\times2}\end{bmatrix}}_{\mathbf{B}_e}\underbrace{\begin{bmatrix}u_d\\ u_q\end{bmatrix}}_{\mathbf{u}} \tag{5}$$

where, $\dot{\xi} = \begin{bmatrix}\dot{\xi}_d\\ \dot{\xi}_q\end{bmatrix}$, $\mathbf{0}_{2\times2}$ is a 2×2 zero matrix, and $\mathbf{I}_2$ is a 2×2 identity matrix.

(5) shows that the system is converted into a linear and fully decoupled system. However, it has two unmeasured states ($\begin{bmatrix}\xi_d & \xi_q\end{bmatrix}$). These states will be estimated and compensated online using KFA.

III. PROPOSED ADAPTIVE CONTROL TECHNIQUE

A. DISTURBANCE ESTIMATION

In this study, KFA is adopted and used to achieve the function of state (disturbance) estimation because it has an accurate and robust response compared to other state observers when the system is exposed to noise, disturbances, and uncertainties [28]. KFA is an adaptive observer that is used to estimate states in linear systems. KFA consists of two sequential steps. The first one is responsible for the prediction, while the other one performs measurements and states updates [29].

The estimation process is done based on the error variance and covariance matrices. The main advantage of KFA is that it does not require parameter or gain tuning. Instead, only states initialization is required. KFA can be summarized as follows [29];

i) Prediction step,

$$\hat{\mathbf{x}}_{ek}^{-} = \mathbf{A}_{ed}\hat{\mathbf{x}}_{ek-1} + \mathbf{B}_{ed}\mathbf{u}_{ek-1} \tag{6}$$

$$\mathbf{P}_k^{-} = \mathbf{A}_{ed}\mathbf{P}_{k-1}\mathbf{A}_{ed}^T + \mathbf{Q}_k \tag{7}$$

ii) Updating step,

$$\mathbf{K}_k = \mathbf{P}_k^{-}\mathbf{H}^T\left(\mathbf{H}\mathbf{P}_k^{-}\mathbf{H}^T + \mathbf{R}_k\right)^{-1} \tag{8}$$

$$\hat{\mathbf{x}}_{ek} = \hat{\mathbf{x}}_{ek}^{-} + \mathbf{K}_k\left(\mathbf{z}_k - \mathbf{H}\hat{\mathbf{x}}_{ek}^{-}\right) \tag{9}$$

$$\mathbf{P}_k = \left(\mathbf{I} - \mathbf{K}_k\mathbf{H}\right)\mathbf{P}_k^{-} \tag{10}$$

where, $\mathbf{A}_{ed}$ and $\mathbf{B}_{ed}$ are the discrete state matrix and the input matrix shown in (13) and (14), $\hat{\mathbf{x}}_{ek}$ is the vector of discrete estimated states, $\mathbf{u}_k$ is the vector of discrete inputs, $\mathbf{P}_k$ is the estimation error covariance matrix, $\mathbf{Q}_k$ is the process noise covariance matrix, $\mathbf{K}_k$ is Kalman gain, $\mathbf{H}$ is the output matrix, $\mathbf{R}_k$ is the noise covariance error, $\mathbf{z}_k$ is the measurement vector, $\mathbf{I}$ is the identity matrix, and $(.^{-})$ denotes to the value before the estimation. The dynamic model described in (5) must be discretized to make it suitable for KFA. The discretization process can be done using Euler's Method,

$$\mathbf{A}_{ed} = \mathbf{I} + \mathbf{T}_s.\mathbf{A}_e \tag{11}$$

$$B_{ed} = T_s.\mathbf{B}_e \tag{12}$$

where T_s is the sampling time, $\mathbf{A}_{ed}$ and $\mathbf{B}_{ed}$ are shown in (13) and (14) respectively. Finally, (5) is discretized using (11) and (12) as follows,

$$\mathbf{A}_{ed} = \begin{bmatrix}1 - \frac{RT_s}{L} & 0 & T_s & 0\\ 0 & 1 - \frac{RT_s}{L} & 0 & T_s\\ 0 & 0 & 1 & 0\\ 0 & 0 & 0 & 1\end{bmatrix} \tag{13}$$

$$\mathbf{B}_{ed} = \begin{bmatrix}-\frac{T_s}{L} & 0\\ 0 & -\frac{T_s}{L}\\ 0 & 0\\ 0 & 0\end{bmatrix} \tag{14}$$

B. LQR CONTROLLER DESIGN

The linear controller represents the second layer of the proposed controller.

The LQR control law is given by,

$$\mathbf{u}_{i0} = -\mathbf{K}\mathbf{e}_{dq} \tag{15}$$

where,

$\mathbf{u}_{i0}$: is the current stabilizer control law.

$\mathbf{K}$: is 2×2 matrix gain.

$\mathbf{e}_{dq}$: is the current tracking error, and given by,

$$\mathbf{e}_{dq} = \begin{bmatrix}e_d\\ e_q\end{bmatrix} = \begin{bmatrix}I_d - I_d^*\\ I_q - I_q^*\end{bmatrix} \tag{16}$$

As the system shown in (4) is decoupled, the gain matrix can be selected as follows,

$$\mathbf{K} = \begin{bmatrix}k_{11} & 0\\ 0 & k_{12}\end{bmatrix} \tag{17}$$

where k_{11} and k_{12} are constants. To select the values of these constants, a Lyapunov function is defined as follows,

$$V = \frac{1}{2}e_d^2 + \frac{1}{2}e_q^2 \tag{18}$$

The derivative of the Lyapunov function can be written as,

$$\dot{V} = e_d\dot{e}_d + e_q\dot{e}_q \tag{19}$$

Assuming that the error between the reference signal and measured signal is small when control law in (15) is used, (4) can be linearized around $\mathbf{e}_{dq} = 0$,

$$\dot{\mathbf{e}}_{dq} \approx \mathbf{A}\mathbf{e}_{dq} + \mathbf{B}\mathbf{u}_{i0} \tag{20}$$

By substituting (20), (4), and (15) in (19), the derivative of the Lyapunov function becomes,

$$\dot{V} = \underbrace{\frac{k_{11}}{L}e_d^2}_{T_1} \underbrace{-\frac{R}{L}e_q^2 - \frac{R}{L}e_d^2}_{T_2} + \underbrace{\frac{k_{22}}{L}e_q^2}_{T_3} \tag{21}$$

It can be noticed from (21) that the term T_2 is negative because R and L are positive. Similarly, T_1 and T_3 are negative if k_{11} and $k_{22} < 0$.

For simplicity, let $k_{11} = -1$ and $k_{22} = -1$, then, the control law can be written as follows,

$$\mathbf{u}_{i0} = \begin{bmatrix} I_d - I_d^* \\ I_q - I_q^* \end{bmatrix} \tag{22}$$

The relation between AC and DC sides quantities of the T-type rectifier can be obtained based on the input and output power balance as follows [5],

$$C\dot{V}_{dc} = 3\frac{V_d I_d + V_q I_q}{V_{dc}} - \frac{V_{dc}}{R_l} \tag{23}$$

When the grid is operating normally, the term $V_q I_q \rightarrow 0$, which means that the DC link voltage is almost not affected by the q part of (23). Therefore, it can be simplified as,

$$C\dot{V}_{dc} = 3\frac{V_d I_d}{V_{dc}} - \frac{V_{dc}}{R_l} \tag{24}$$

(24) shows that the DC link voltage is directly controlled using I_d. However, I_d is controlled directly using (22). Therefore, to regulate the DC link voltage, an additional term will be added to the control law as follows,

$$\mathbf{u}_{i1} = \begin{bmatrix} e_d - e_V \\ e_q \end{bmatrix} \tag{25}$$

where e_V is the DC link voltage tracking error and given by $V_{dc}^* - V_{dc}$.

Another critical control objective for the T-type rectifier is the capacitors' voltages balancing. The method used in [10] is adopted to achieve the balance due to its simplicity. Therefore, the control law becomes,

$$\mathbf{U}_L = \begin{bmatrix} e_d - e_V - k_c \Delta V_c \\ e_q \end{bmatrix} \tag{26}$$

where k_c is a positive constant and ΔV_c is the difference between capacitors' voltages.

C. REFERENCE SIGNALS GENERATION

Traditionally, the error in the DC link voltage is used to generate the reference currents in cascaded control. However, this paper does not depend on the cascaded control topology. The reference current can be computed based on the principle of power balancing between the input and the output sides as follows,

$$\begin{bmatrix} I_d^* \\ I_q^* \end{bmatrix} = \begin{bmatrix} \frac{V_{dc}^{*2}}{\sqrt{3}\, V_d R_L} \\ 0 \end{bmatrix} \tag{27}$$

Generating a current reference signal requires the knowledge of the load resistance. This can be computed using Ohm's law or using the power balance formula, as follows,

$$R_L = \frac{V_{dc}^2}{\sqrt{3}\, V_d I_d} \tag{28}$$

Voltage reference can be generated by the operator. The operator can be a user or a charge controller. Many applications require smooth and timely control of the voltage profile. In these applications, the slope of the voltage should be controllable. To ensure timely and smooth DC link voltage tracking, the reference signal provided by the operator is converted into a signal that is a function of time. This signal should meet the following constraints,

$$V_{dc}\Big|_{t=t_0} = v_i, \quad V_{dc}\Big|_{t=t_f} = V_{dc}^* \tag{29}$$

$$\dot{V}_{dc}\Big|_{t=t_0} = 0, \quad \dot{V}_{dc}\Big|_{t=t_f} = 0 \tag{30}$$

$$\ddot{V}_{dc}\Big|_{t=t_0} = 0, \quad \ddot{V}_{dc}\Big|_{t=t_f} = 0, \tag{31}$$

where v_i is the initial voltage, t is the instant time, and t_f is the desired transient time.

These six constraints can be achieved if the reference voltage profile is designed as a 5^{th}-order polynomial as follows,

$$V_{dc}^*(t) = a_5 t^5 + a_4 t^4 + a_3 t^3 + a_2 t^2 + a_1 t + a_0 \tag{32}$$

By substituting the constraints in (32), the constants a_5 to a_0 can be computed as follows,

$$\begin{aligned} a_0 &= a_1 = a_2 = 0, \quad a_3 = \frac{10}{t_f^3}(v_f - v_i) \\ a_4 &= \frac{-15}{t_f^4}(v_f - v_i), \quad a_5 = \frac{6}{t_f^5}(v_f - v_i) \end{aligned} \tag{33}$$

To generate the explicit control law, substitute (33) and (27) in (26),

$$\mathbf{U}_L = \begin{bmatrix} I_d - \frac{V_{dc}^{*2}}{\sqrt{3}\, V_d R_L} - V_{dc}^*(t) + V_{dc} - k_c \Delta V_c \\ I_q \end{bmatrix} \tag{34}$$

Finally, the standard dq three-phase PLL function [30] is used to estimate the phase angle. The overall block diagram and control flow chart of the proposed control scheme are shown in Fig.2.

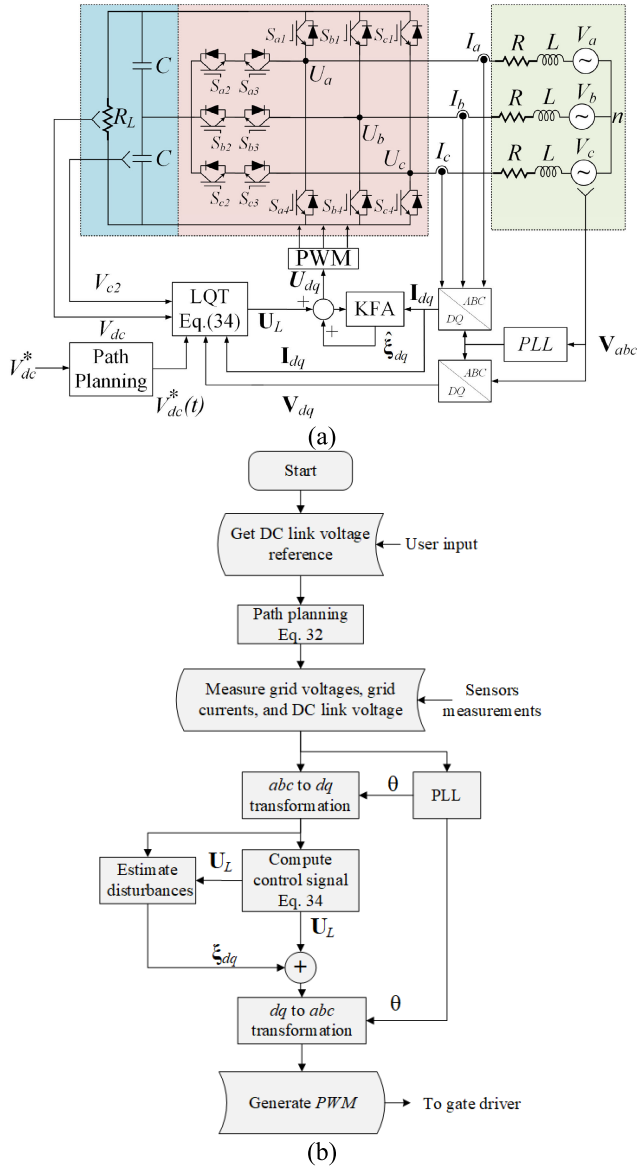

FIGURE 2. (a) Block diagram of the proposed control method (b) Control process flow chart.

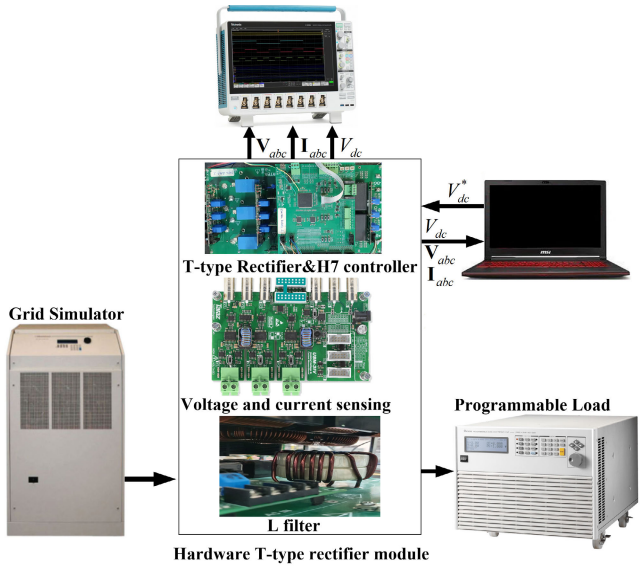

FIGURE 3. Experimental setup for three-phase T-type rectifier.

IV. SIMULATION AND EXPERIMENTAL RESULTS

The adaptivity and robustness of the proposed control scheme were validated by a series of experiments carried out on a hardware prototype shown in Fig. 3. The hardware setup consists of California Instrument MX30 regenerative grid simulator as an input source, an L-filter, a lab-scale T-type rectifier, Tektronix oscilloscope to obtain experiment results, Chroma 63084 programmable electrical load, and STM32H745 dual-core controller to execute the control algorithm.

A. EXPERIMENTAL STEADY-STATE RESULTS

The first experiment was conducted assuming that all system's parameters are well known, including grid voltages, grid resistance, grid inductance, load resistance, filter inductance, and DC capacitors as shown in Table 2. Steady-state experimental results are shown in Fig. 4 (a) and the THD analysis is shown in Fig. 4(b). It is clear from the results that the first control objective (i.e. a sinusoidal line current with a unity power factor) is achieved. The THD of the line currents value is 0.9% which is within the range of international standards. The DC link voltage is 400V with almost zero steady-state error and almost no ripples or oscillations.

TABLE 2. System and control parameters.

Symbol	Value	Symbol	Value
$\mathbf{V}_{abc}$	110 V_{rms}	L	1-5mH
R	$50m\Omega$	C	$1000\mu F$
R_L	$40-20\Omega$	V_{dc}^*	350-400V
T_s	$10\mu s$	t_f	$0.02s$
f_s	10kHz	k_c	0.1

B. EXPERIMENTAL TRANSIENT RESULTS

The transient response of the controller was also validated. A step reference signal was applied to the controller, the initial value was 350V, and the final value was 400V. The transient response is shown in Fig. 5. The response is fast and smooth, with almost no overshoot in the DC link voltage nor in the grid currents. It is evident that the DC voltage and grid's currents converge to the desired value within the desired time ($t_f = 0.02$s).

Another experiment was conducted by increasing the load suddenly, as shown in Fig. 6. The load was changed from 2.67 kW to 8 kW. This was done by changing the resistance of the load from 40 to 20Ω, while the reference voltage of the dc-link was adjusted to 400V. Although the load has 100% of sudden change, only a small voltage drop occurs in the DC link voltage, which represents less than 2.5%. However, the controller was fast and able to compensate the drop during one cycle.

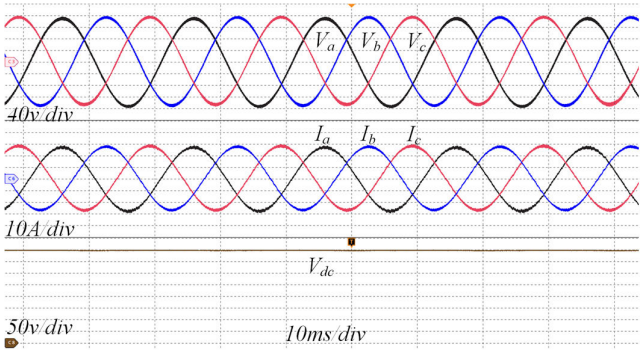

(a)

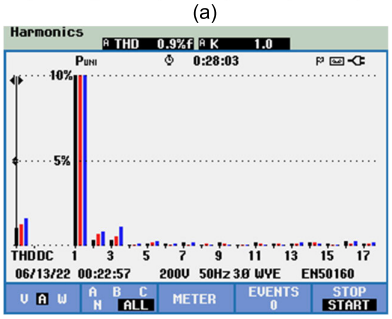

(b)

FIGURE 4. Experimental results of the steady-state analysis. (a) Steady state response. (b) Grid currents THD.

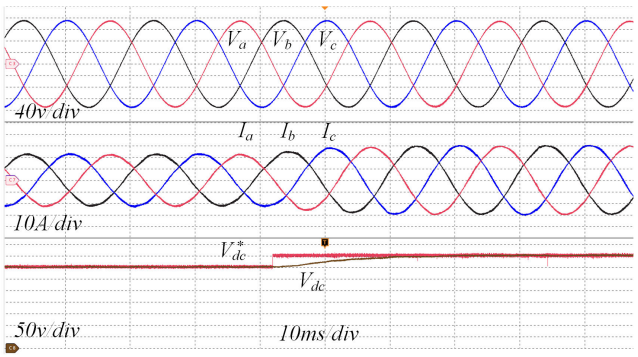

FIGURE 5. Experimental results of transient response using the well-known model.

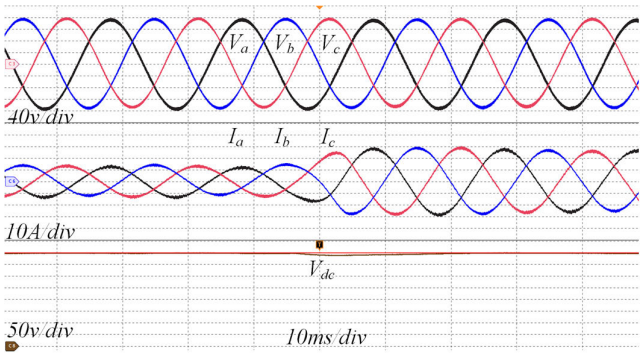

FIGURE 6. Experimental results of the rectifier under 100% load change.

The current moved from the initial value to the final value smoothly and immediately without any overshooting or oscillation. This is thanks to the fast and adaptive response of the KFA, for which the difference in the load resistance is considered a disturbance. Then KFA estimates and compensates its effect along with the other disturbances.

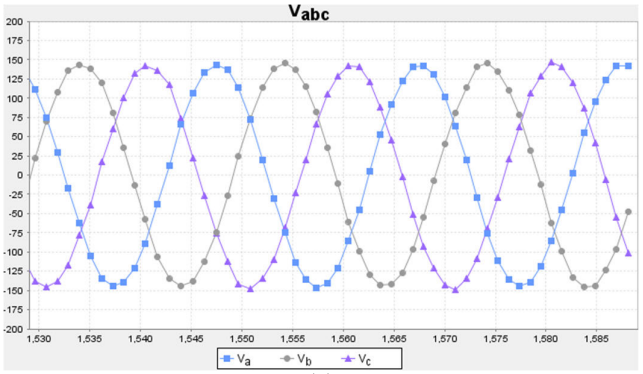

(a)

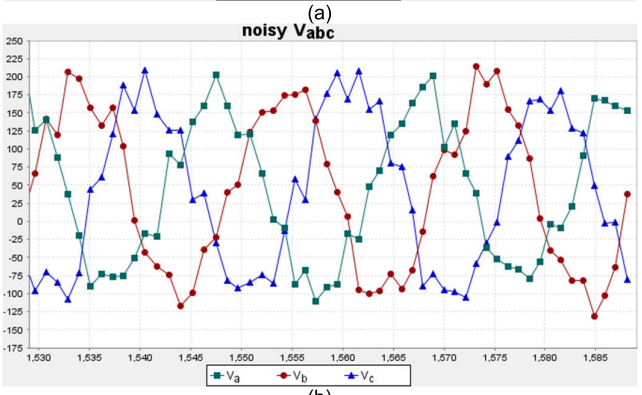

(b)

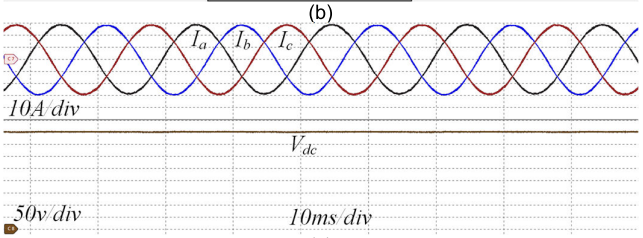

(c)

FIGURE 7. Experimental results of the rectifier under grid voltage measurement noise. (a) grid voltages (b) Noisy grid voltages mesurements. (c) generated grid currents.

C. EXPERIMENTAL ANALYSIS OF SYSTEM UNCERTAINTIES

Industrial rectifiers are usually exposed to measurement noises, especially those used for high power. To test the adaptivity of the proposed controller against noises, a random noise signal was added to the voltage measurement, as shown in Fig.7. The generated noise has a maximum amplitude $\pm 50V$ representing about 50% of the measurement. This noise is considered high, but it represents a good challenge to prove the robustness of the controller against noise. The noisy voltages were acquired using STMStudio software because the noise was generated programmatically inside the microcontroller and cannot be shown by the oscilloscope. The resulted noisy measurements, the DC link voltage, and grid currents are shown in Fig.7 (b) and (c). The figure shows that the response is almost not affected, and the current is kept smooth, sinusoidal, and has a unity power factor.

The performance of the DC voltage tracking did not change too, where the output DC voltage is constant, with no ripple, and with zero steady-state error. Fig.8 shows the response of the controller to a distorted input voltage. In this experiment, a 7% fifth-order harmonic component and a 5% seventh-order harmonic component are added to the grid voltages as shown in Fig.8(b). Fig.8 shows that the DC link voltage is almost not affected by the distorted input voltage. The generated grid currents are still in phase with grid voltages, the THD of the grid currents is increased to 3.4% as shown in Fig.8 (c). However, the obtained THD is still within the range of international standards.

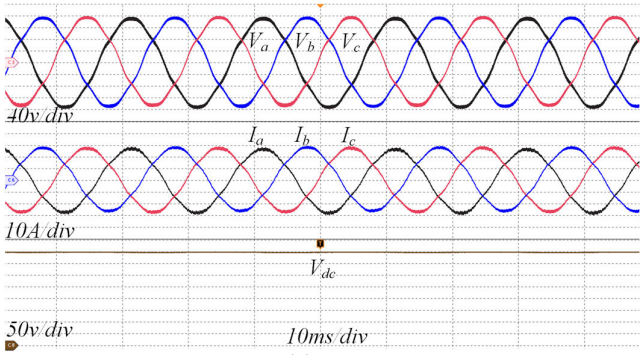

(a)

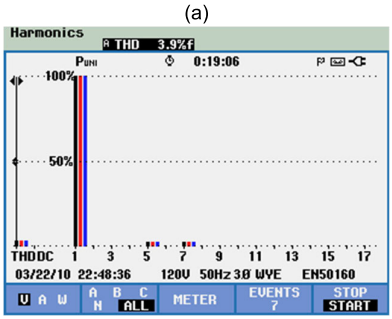

(b)

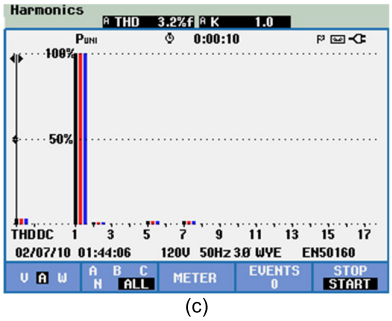

(c)

FIGURE 8. Experimental results of the rectifier under distorted grid voltage. (a) Grid voltages, grid currents, and DC link voltage. (b) Input voltage THD results. (c) Input current THD results.

The controller was validated under the condition of unbalanced grid voltage, as shown in Fig.9. The voltages of phases were adjusted to $100\sqrt{2}$, $110\sqrt{2}$, and $120\sqrt{2}$. Even if there is a 9.1% grid voltage unbalance, the grid currents are slightly affected, the unbalance ratio between the currents is 2.72%. At the same time, the power factor remains unaffected. The ripple in the DC link voltage is slightly affected, where the value of peak-to-peak ripple voltage (V_{rpp}) is 7.53V

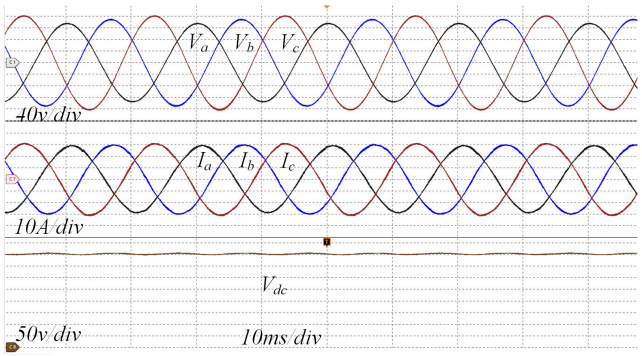

FIGURE 9. Experimental results of the rectifier under unbalanced grid voltage.

TABLE 3. System parameters and uncertainty percentage.

Symbol	Value	Uncertainty
R	$200\,m\,\Omega$	400%
R_l	$20\,\Omega$	200%
L	$5\,m\,H$	500%

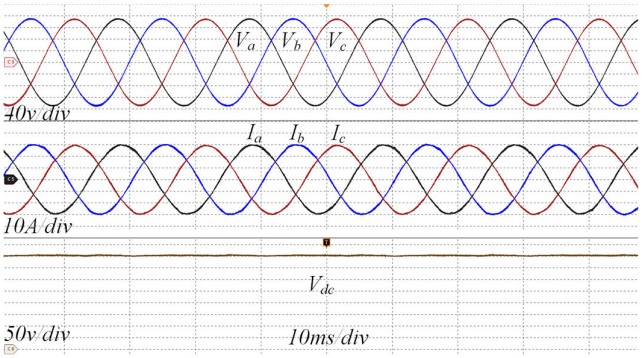

FIGURE 10. Steady-state response of the rectifier under high uncertainty.

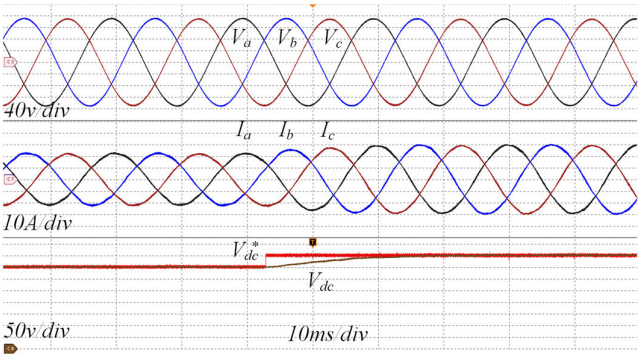

FIGURE 11. Transient response of the rectifier under severe uncertainty.

which represents 1.88% of the output voltage. However, the obtained V_{rpp} is within the international standards.

The validity of the controller was ensured under normal and abnormal conditions, where the system was exposed to external noise, unbalanced grid voltage, and sudden load change. However, the main purpose of this controller is to

achieve the same results under high uncertainty conditions. Therefore, a severe uncertainty is added to the model.

The uncertainty is achieved by changing the values of the system's components (inductance, capacitance, and load resistance) without changing the gains of the controller. The new parameters and uncertainty amount are shown in Table 3. This high uncertainty level is considered because industrial rectifiers may deal with a wide range of loads. Fig.10 shows the steady state response of the proposed controller during these conditions. It can be noticed that the the effects of the uncertainties are compensated by the KFA, and the response is almost not affected, even if a high range of uncertainty is considered. The output voltage is well regulated with no steady-state errors, and the power factor is maintained unity. The robustness of the proposed controller has been achieved to the adaptive and robust response of the KFA algorithm, where all uncertainties are assumed as disturbances and compensated by the first layer rapidally.

The transient response of the controller under a high range of uncertainty is shown in Fig.11. The DC link voltage converged smoothly and rapidly to the reference signal. It can be noticed that the steady-state error is about zero, with no overshoot and no voltage ripples. The grid currents are changed from the initial value to the final value smoothly with no overshoot.

This experiment ensures the validity and robustness of the proposed controller under the effect of a high uncertainty range. It is the evident that the controller is able to achieve the required steady-state and transient behavior efficiently, even when the uncertainty is severe.

D. SIMULATION COMPARISON STUDY

To prove the advantages of the ACT controller over the existing, three studies are adopted for comparison. The first one is the passivity-based control proposed in [25]. Passivity-based control is selected for the comparison as it depends on a single-loop control instead of the cascaded control. The second one is a disturbance rejection control based on H∞ controller proposed in [26]. The third is the SMC proposed in [10]. Fig. 12 shows the simulation results for PBC, H∞, SMC, and ACT controllers, respectively. The comparison study includes four stages of online changes as follows,

A. Steady state period (0.02s – 0.07s): the reference voltage is set to 350V, load resistance is 40Ω, and filter's inductance is 1mH.

B. Transient period (0.07s – 0.12s): the reference voltage is increased to 400V, load resistance is 40Ω, and filter's inductance is 1mH.

C. Online load change (0.12s – 0.17s): the load resistance is changed online from 40Ω to 20Ω, the reference voltage is 400V, and filter's inductance is 1mH.

D. Input filter parameters change (0.17s – 0.22s): the inductance of the input filter is increased to 5mH, the reference voltage is 400V, and the load resistance is 20Ω

The first two periods aim to prove that all controllers are well-designed and the parameters of PBC and H∞ are well calibrated for both transient and steady state periods. The other two periods aim to compare the robustness of the controllers against load and input filter's inductance change. The PBC and H∞ controllers were designed and tuned to provide the best possible performance for the parameters defined in the periods A and B. Then, the load resistance and filter's inductance are changed online without changing any parameter in all controllers.

TABLE 4. Comparison results among controllers.

Controller	PBC	H∞	SMC	ACT
Steady-state error	High	Low	Low	Low
Tuning process	Simple	Complex	Simple	Simple
Current overshoot	Low	High	High	Low
Voltage overshoot	Low	Mid	Mid	Low
Control loops	Single	cascaded	Cascaded	Single
THD	0.8%	1.75%	1.1%	0.75%
Robustness to load change	Low	High	High	High
Robustness to filter change	High	Low	Low	High

During the steady-state period, all controllers show excellent response represented by a unity power factor, no ripples in the DC link voltage, and low THD. However, the PBC has a steady state error (11.4%) in the DC link voltage due to the open-loop generation of the reference currents. In the next period, the reference DC link voltage is stepped up from 350V to 400V. For PBC, the tracking error still exists in the DC link voltage, and the transient time is larger than the other controllers because the DC link voltage is not controlled directly by the control law. The H∞ and SMC achieved fast and accurate tracking for the reference signal. However, both of them have high overshoot in both grid currents and DC link voltage. The ACT shows excellent transient behavior, where the tracking is done accurately and smoothly. When the load is changed, all controllers compensate the effect of the load step. However, the steady-state error vanishes for the PBC when the load is changed to 20Ω. Finally, when the inductance of the input filter is changed online to 5mH, the response of the H∞ is deteriorated, the ripples in the DC link voltage are noticeably increased, and the grid currents become highly distorted. For the SMC, the chattering problem appears in the grid currents and becomes reflected on the DC link voltage, where a high frequency ripple appears on the DC link voltage and the grid currents deteriorated. The PBC shows better performance against filter changes, the DC link voltage is dropped (1.85%) for a while then it is restored with some ripple at the steady state. The proposed ACT shows excellent response for filter's inductance change. At the instant of change, the DC link voltage is dropped (less than 1%) and compensated directly, while the grid currents are almost not affected.

In summary, the PBC response shows that it is suitable for a specific load (20Ω), but a noticeable steady state error appears for another load (40 Ω). The response of H∞ and

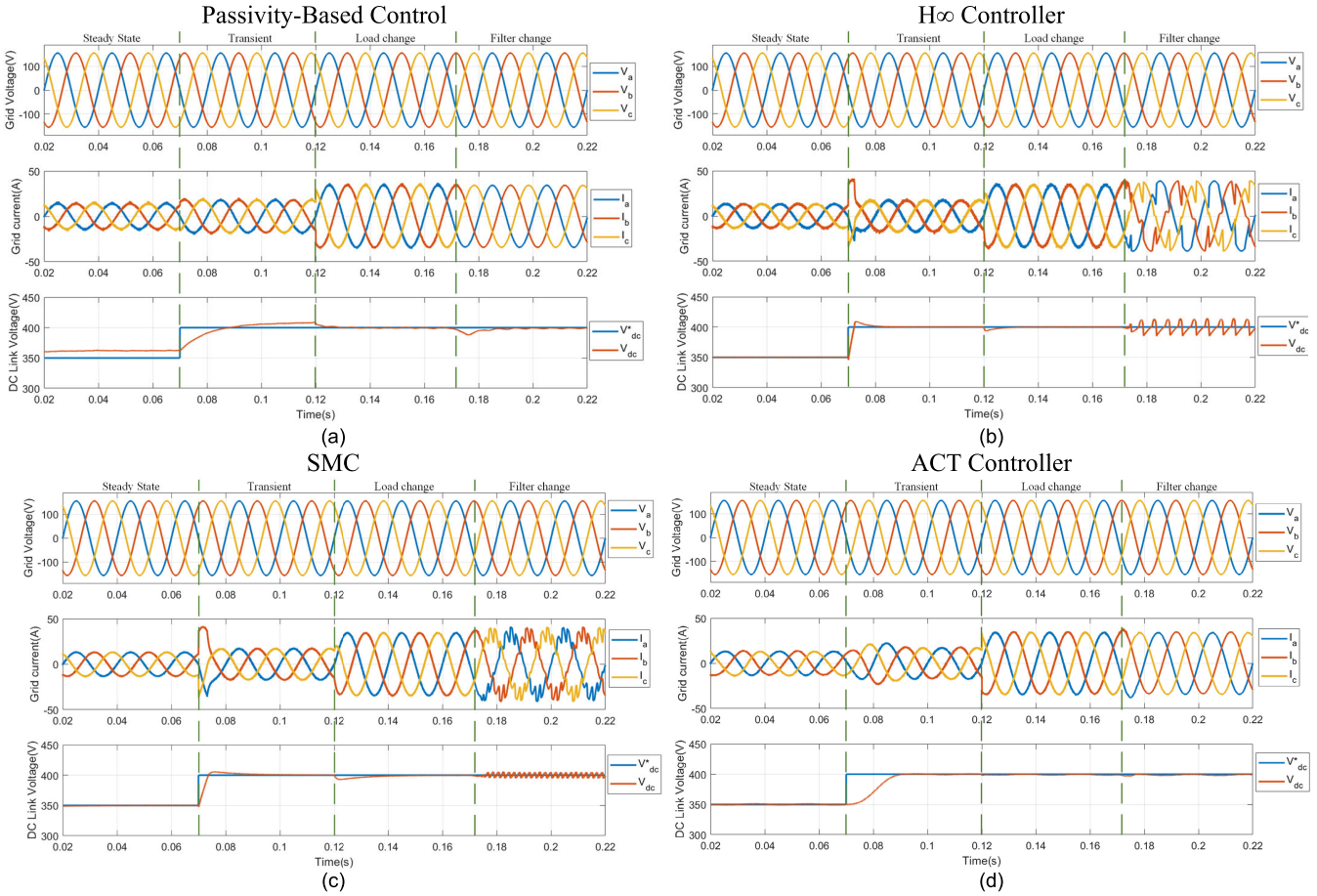

FIGURE 12. Simulation results during steady state, transient, sudden load change, and filter's parameters change (1) PBC (2) H∞ (3) SMC (4) ACT.

SMC is satisfactory with current and voltage overshoot for a specific inductance of input filter (1 mH), but the response is deteriorated for different inductance value (5mH) and the chattering problem appears in the SMC. The proposed ACT controller shows excellent response for steady state, transient, load change, and filter's inductance change. The H∞ and the PBC can be re-tuned to obtain excellent response for the new values, but they need to be re-tuned at each time when the parameters are changed. In the proposed ACT, no need to tune or change any variable regardless the amount of the uncertainty as it will be compensated by the KFA. The results of this comparison are shown in Table 4.

V. CONCLUSION

An adaptive controller for a three-phase three-level T-type rectifier was proposed and analyzed in this paper. The proposed controller consists of two layers; the first one is responsible for compensating nonlinearities, uncertainties, disturbances, and coupling effects between system's states. The second layer is a linear controller that is responsible for controlling both DC link voltage and grid currents.

The proposed controller showed an adaptive, robust, fast, accurate, and smooth response. It was proved in the paper that the proposed controller could effectively deal with high measurement noise, high uncertainties, and high disturbances, including a 100% sudden load change, unbalanced grid voltages, distorted input voltage, and severe parameter change.

ACKNOWLEDGMENT

The statements made herein are solely the responsibility of the authors.

REFERENCES

[1] D. Shahzad, S. Pervaiz, N. A. Zaffar, and K. K. Afridi, "GaN-based high-power-density AC–DC–AC converter for single-phase transformerless online uninterruptible power supply," *IEEE Trans. Power Electron.*, vol. 36, no. 12, pp. 13968–13984, Dec. 2021.

[2] L. Huang, A. Murray, and B. Flynn, "A high-efficiency low-power rectifier for wireless power transfer systems of deep micro-implants," *IEEE Access*, vol. 8, pp. 204057–204067, 2020.

[3] H. Zhao, Y. Shen, W. Ying, S. S. Ghosh, M. R. Ahmed, and T. Long, "A single- and three-phase grid compatible converter for electric vehicle on-board chargers," *IEEE Trans. Power Electron.*, vol. 35, no. 7, pp. 7545–7562, Jul. 2020.

[4] M. A. Omar and M. M. Mahmoud, "Control of power converter used for electric vehicle DC charging station with the capability of balancing distribution currents and reactive power compensation," *Int. J. Power Electron. Drive Syst.*, vol. 12, no. 2, p. 924, Jun. 2021.

[5] D. Cittanti, M. Gregorio, E. Bossotto, F. Mandrile, and R. Bojoi, "Full digital control and multi-loop tuning of a three-level T-type rectifier for electric vehicle ultra-fast battery chargers," *Electronics*, vol. 10, no. 12, p. 1453, Jun. 2021.

[6] Z. Song, Y. Tian, Z. Yan, and Z. Chen, "Direct power control for three-phase two-level voltage-source rectifiers based on extended-state observation," *IEEE Trans. Ind. Electron.*, vol. 63, no. 7, pp. 4593–4603, Jul. 2016.
[7] Y. Liu, W. Zhang, J. Lin, M. Su, and X. Liang, "Active power decoupling control for single-phase current source rectifier based on emulating LC resonator," *IEEE Trans. Ind. Electron.*, vol. 68, no. 6, pp. 5460–5465, Jun. 2021.
[8] L. Ming, W. Ding, P. C. Loh, and Z. Xin, "A direct carrier-based modulation scheme with full index range for DC-link current ripple mitigation of a current source converter," *IEEE Trans. Ind. Electron.*, vol. 69, no. 1, pp. 452–462, Jan. 2022.
[9] C. Sui, Y. He, and M. Chen, "Analysis of current distortion of three-phase voltage source rectifiers and its application in fault diagnosis," *IEEE Access*, vol. 8, pp. 4065–4075, 2020.
[10] S. Bayhan and H. Komurcugil, "Sliding-mode control strategy for three-phase three-level T-type rectifiers with DC capacitor voltage balancing," *IEEE Access*, vol. 8, pp. 64555–64564, 2020.
[11] X. Zhang, G. Tan, T. Xia, Q. Wang, and X. Wu, "Optimized switching finite control set model predictive control of NPC single-phase three-level rectifiers," *IEEE Trans. Power Electron.*, vol. 35, no. 10, pp. 10097–10108, Oct. 2020.
[12] P. Zhang, X. Wu, W. Xu, J. Liu, J. Qi, and A. Yang, "A compensation component injection method based on a hybrid modulation for minimizing the neutral-point voltage oscillations in a five-level flying capacitor rectifier," *IEEE Trans. Power Electron.*, vol. 37, no. 3, pp. 2705–2718, Mar. 2022.
[13] J. Wang, X. Yuan, and B. Jin, "Carrier-based closed-loop DC-link voltage balancing algorithm for four level NPC converters based on redundant level modulation," *IEEE Trans. Ind. Electron.*, vol. 68, no. 12, pp. 11707–11718, Dec. 2021.
[14] P. Karamanakos, K. Pavlou, and S. Manias, "An enumeration-based model predictive control strategy for the cascaded H-bridge multilevel rectifier," *IEEE Trans. Ind. Electron.*, vol. 61, no. 7, pp. 3480–3489, Jul. 2014.
[15] M. Babaie, M. Mehrasa, M. Sharifzadeh, and K. Al-Haddad, "Floating weighting factors ANN-MPC based on Lyapunov stability for seven-level modified PUC active rectifier," *IEEE Trans. Ind. Electron.*, vol. 69, no. 1, pp. 387–398, Jan. 2022.
[16] S. Yan, Y. Yang, S. Y. Hui, and F. Blaabjerg, "A review on direct power control of pulsewidth modulation converters," *IEEE Trans. Power Electron.*, vol. 36, no. 10, pp. 11984–12007, Oct. 2021.
[17] P. Maciejewski and G. Iwanski, "Study on direct torque control methods of a doubly fed induction machine working as a stand-alone DC voltage generator," *IEEE Trans. Energy Convers.*, vol. 36, no. 2, pp. 853–862, Jun. 2021.
[18] J.-S. Lee and K.-B. Lee, "An open-switch fault detection method and tolerance controls based on SVM in a grid-connected T-type rectifier with unity power factor," *IEEE Trans. Ind. Electron.*, vol. 61, no. 12, pp. 7092–7104, Dec. 2014.
[19] G. Mirzaeva, G. C. Goodwin, B. P. McGrath, C. Teixeira, and M. E. Rivera, "A generalized MPC framework for the design and comparison of VSI current controllers," *IEEE Trans. Ind. Electron.*, vol. 63, no. 9, pp. 5816–5826, Sep. 2016.
[20] B. Chelladurai, C. K. Sundarabalan, S. N. Santhanam, and J. M. Guerrero, "Interval type-2 fuzzy logic controlled shunt converter coupled novel high-quality charging scheme for electric vehicles," *IEEE Trans. Ind. Informat.*, vol. 17, no. 9, pp. 6084–6093, Sep. 2021.
[21] J. Liu, X. Sun, B. Ren, W. Song, and P. Wheeler, "Strong adaptability control based on dual-division-summation current control for an LCL-type grid-connected inverter," *IEEE Trans. Power Electron.*, vol. 37, no. 12, pp. 14157–14172, Dec. 2022.
[22] R. Guzman, L. G. de Vicuña, M. Castilla, J. Miret, and H. Martin, "Variable structure control in natural frame for three-phase grid-connected inverters with LCL filter," *IEEE Trans. Power Electron.*, vol. 33, no. 5, pp. 4512–4522, May 2018.
[23] B. Long, P. J. Lu, K. T. Chong, J. Rodriguez, and J. Guerrero, "Robust fuzzy-fractional-order nonsingular terminal sliding-mode control of LCL-type grid-connected converters," *IEEE Trans. Ind. Electron.*, vol. 69, no. 6, pp. 5854–5866, Jun. 2022.
[24] E. T. Andrew, K. H. Ahmed, and D. Holliday, "A new model predictive current controller for grid-connected converters in unbalanced grids," *IEEE Trans. Power Electron.*, vol. 37, no. 8, pp. 9175–9186, Aug. 2022.
[25] H. Komurcugil, S. Bayhan, and M. Malinowski, "Passivity-based control strategy with improved robustness for single-phase three-level T-type rectifiers," *IEEE Access*, vol. 9, pp. 59336–59344, 2021.
[26] Y. Yin, J. Liu, W. Luo, L. Wu, S. Vazquez, J. I. Leon, and L. G. Franquelo, "Adaptive control for three-phase power converters with disturbance rejection performance," *IEEE Trans. Syst., Man, Cybern. Syst.*, vol. 51, no. 2, pp. 674–685, Feb. 2021.
[27] P. Alemi, S.-Y. Jeong, and D.-C. Lee, "Active damping of LLCL filters using PR control for grid-connected three-level T-type converters," *J. Power Electron.*, vol. 15, no. 3, pp. 786–795, May 2015.
[28] I. Hashlamon, "Adaptive disturbance estimation and compensation for delta robots," *Jordan J. Mech. Ind. Eng.*, vol. 14, no. 4, pp. 413–422, 2020.
[29] I. Hashlamon and K. Erbatur, "An improved real-time adaptive Kalman filter with recursive noise covariance updating rules," *TURKISH J. Electr. Eng. Comput. Sci.*, vol. 24, no. 2, pp. 524–540, 2016.
[30] S. S. Refaat, O. Ellabban, S. Bayhan, H. Abu-Rub, F. Blaabjerg, and M. M. Begovic, *Smart Grid and Enabling Technologies*. Hoboken, NJ, USA: Wiley, 2021.

ALI SHARIDA (Student Member, IEEE) received the B.E. degree in mechatronics engineering from Palestine Technical University (PTUK), Tulkarm, Palestine, in 2013, and the M.Sc. degree in mechatronics engineering from Palestine Polytechnic University (PPU), Hebron, Palestine, in 2020. He is currently pursuing the Ph.D. degree with Texas A&M University at Qatar. In 2014, he joined PTUK as a T.A. In 2022, he was with Texas A&M University at Qatar as an Associate Research Assistant. His current research interests include robotics modeling and design, motion control, intelligent systems, systems identification, power converters, PWM rectifier control, and adaptive control.

SERTAC BAYHAN (Senior Member, IEEE) received the bachelor's, M.S., and Ph.D. degrees in electrical engineering from Gazi University, Ankara, Turkey, in 2008 and 2012, respectively.

His research interests include power electronics and their applications in next-generation power and energy systems, including renewable energy integration, electrified transportation, and demand-side management. He has acquired $13M in research funding and published more than 170 papers in mostly prestigious IEEE journals and conferences. He is also the coauthor of three books and six book chapters. He currently serves as an Associate Editor for IEEE TRANSACTIONS ON INDUSTRIAL ELECTRONICS, IEEE JOURNAL OF EMERGING AND SELECTED TOPICS IN INDUSTRIAL ELECTRONICS, IEEE OPEN JOURNAL OF THE INDUSTRIAL ELECTRONICS SOCIETY, and IEEE Industrial Electronics Technology News, and the Guest Editor for the IEEE TRANSACTIONS ON INDUSTRIAL INFORMATICS.

HAITHAM ABU-RUB (Fellow, IEEE) received the M.Sc. degree in electrical engineering from Gdynia Maritime Academy, Gdynia, Poland, 1990, the Ph.D. degree in electrical engineering from the Gdańsk University of Technology, Poland, in 1995, and the Ph.D. degree in humanities from Gdańsk University, Gdańsk, Poland, in 2004. Since 2006, he has been with Texas A&M University at Qatar, Doha, Qatar, where he is currently a Professor and the Managing Director of the Smart Grid Center Extension. His research interests include energy conversion systems, smart grid, renewable energy systems, electric drives, and power electronic converters. He has coauthored more than 550 journals and conference papers, six books, and six book chapters. He is the Co-Editor-in-Chief of the IEEE TRANSACTIONS ON INDUSTRIAL ELECTRONICS. He was a recipient of many prestigious national and international awards and recognitions, such as the American Fulbright Scholarship and the German Alexander von Humboldt Fellowship.